Supporting Information

Mechanistic Insight of NH_3-assisted Selective Reduction of NO on CeO_2 by A First-principles Microkinetic Study: Selectivity and Activity

Danfeng Xiong[a], Yang Chen[a], Haiyang Yuan[*ab], Haifeng Wang[a]

[a] *Key Laboratory for Advanced Materials, Research Institute of Industrial Catalysis and Center for Computational Chemistry, School of Chemistry and Molecular Engineering, East China University of Science and Technology, Shanghai, 200237, China.*

[b] *Key Laboratory for Ultrafine Materials of Ministry of Education, Shanghai Engineering Research Center of Hierarchical Nanomaterials, School of Materials Science and Engineering, East China University of Science and Technology, Shanghai 200237, China.*

Table S1. The entropy of surface species in the initial/transition/final states corresponding to the steps of $*NH_3$ dissociation and $*NH_2NO$ formation (unit: eV).

Step	Initial state	Transition state	Final state
$*NH_3 + O\# \rightarrow *NH_2 + HO\#$	0.15	0.19	0.18
$*NH_2 + ONO\# \rightarrow *NH_2NO + O\#$	0.25	0.28	0.14

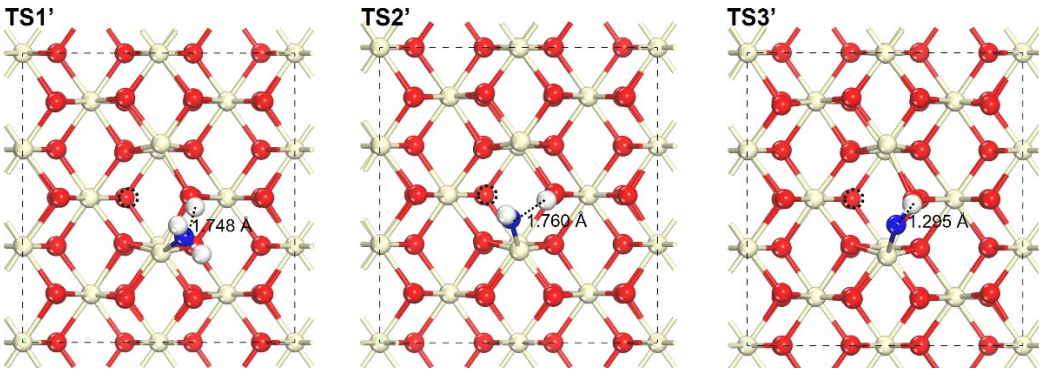

Figure S1. Transition states of the dehydrogenation of *NH_3 (TS1'), *NH_2 (TS2') and *NH (TS3'), assisted by O_{lat} on CeO_2(110) with O_{vac}, respectively. The black dashed circle represents the oxygen vacancy (O_{vac}).

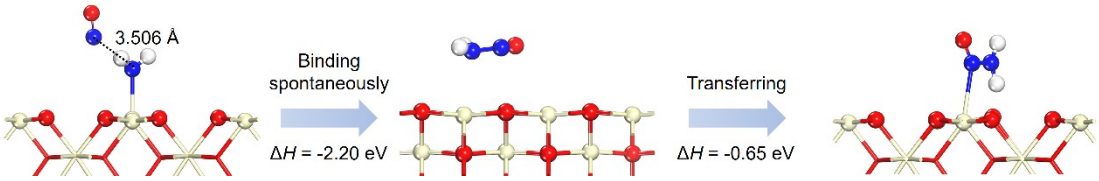

Figure S2. Process of the gaseous NO directly attacking NH_2 on the Ce_{cus} site

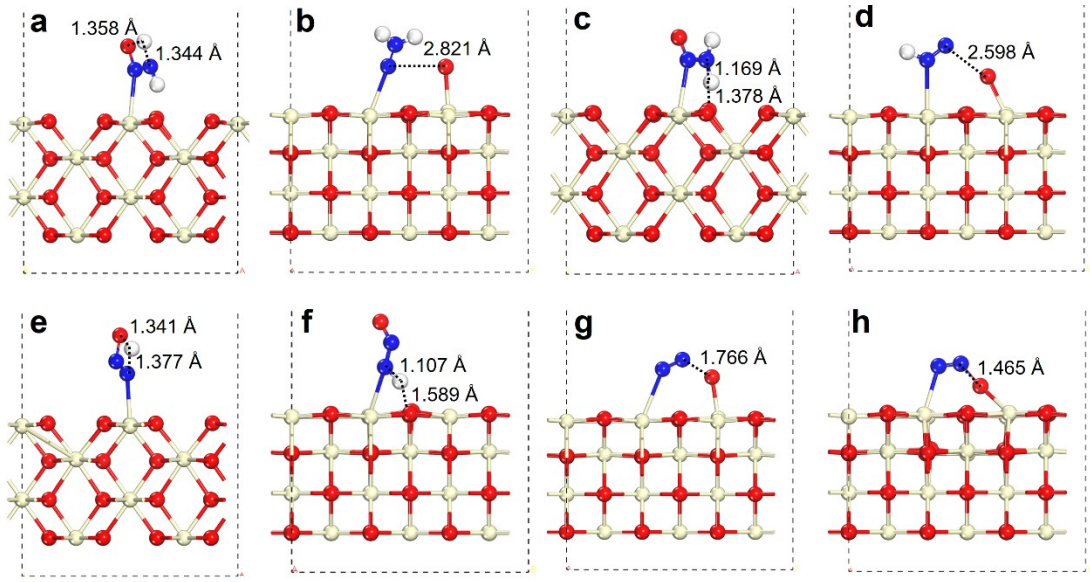

Figure S3. Some transition states in NH_2NO conversion.

Note S1. Kinetic Details

According to the De Donder relation,[1] the net rate for elementary step *i* in terms of the forward rate constant, k_i, the coverage of the reactant on active sites, ϑ(j), and the reversibility, Z_i, can be written as:

$$r_i = k_i \prod_j \theta(j)^{v_{ij}} (1 - Z_i) \quad \text{(Eqn-S1)}$$

where $Z_i = \prod \theta(j)^{v_{ij}} / K_{eq,i}$, which approaches zero as step *i* becomes irreversible and approach unity as step becomes in quasi-equilibrium. $K_{eq,i}$ is the equilibrium constant of step *i*, determined by the standard Gibbs free energy change of the reaction, $K_{eq,i} = \exp(-\Delta G_i/RT)$. v_{ij} are the stoichiometric coefficients for the *j* reactants or products of step *i*. Z_i can be solved by the following the steady state condition. In our micro-kinetic model, the condition that the sum of coverages of adsorbed species on the Ce_{cus} site and the lattice O_{lat} site are equal to 1, respectively. Then, the coverage of all species can be obtained, and the rate of the reaction can be calculated accordingly.

Here, we used the collision theory[2] to estimate the barriers (E_a) of gas-phase molecule adsorption process, as well as the barrier of the gas-phase NO coupling with the surface NH2* species. Therefore, according to the transition state theory and collision theory, the reaction rate on a per site basis can be written as:

$$r_+(T) = \frac{k_B T}{h} \exp(-\frac{E_a}{k_B T}) \frac{P_i}{P^0} \approx S_i(T) \frac{P_i A}{\sqrt{2\pi k_B m_i T}} \quad \text{(Eqn-S2)}$$

where k_B, h, T, P_i and mi are Boltzmann constant, Planck constant, reaction temperature, pressure and the mass of gas molecule, respectively. And, *A* is the area of the atom which is described as $A = \pi r^2$, in which *r* is the VDW radius of the atom. Here, we have assumed that the gas behaves ideally, and $S_i(T)$, the sticking coefficient, is approximated as 1. Hence, we could derive an equation about E_a:

$$E_a \approx -k_B T \ln(\frac{P^0 A h}{k_B T \sqrt{2\pi k_B m_i T}}) \quad \text{(Eqn-S3)}$$

In our microkinetic simulation, the experimental condition for NH_3-SCR on CeO_2, T = 500 K, $P_{NH3} = 5.0\times10^{-4}$ atm, $P_{NO} = 5.0\times10^{-4}$ atm, P_{O2} = 0.03 atm, P_{N2} = 0.8 atm and P_{H2O} = 0.05 atm was used.[3] The microkinetic simulation was carried out by the CATKINAS package,[4-6] in which several powerful self-developed methods solver are illustrated, which mainly include the sensitivity-supervised inter-lock algorithm (SSIA), particle swarm optimization and modified Newton's method coupling system (PNEWCS), and reversibility iteration method (RIM). In the multilevel solver of CATKINAS, these self-developed methods are invoked in a sequence which considers both the speed and the accuracy. For a single-point task, SSIA would be the first choice, despite that common ODEN-A is also provided as it is relatively efficient in quite a few cases. PNEWCS has the best convergence ability, but it is the most time-consuming one. Hence, PNEWCS is placed at the end of the multilevel solver in case all the other methods fail to converge. Variable step size algorithm is used, which can automatically adjust to a maximum step size to meet the convergence criteria according to the

algorithm; if the change is large, the step size will be very small. The MATLAB random number generator is initialized by using the default algorithm and seed.

Note S2. Calculation for Phase diagram of CeO_2(110)

The saturation of each Ce site on the surface is closely related to the coverage of O species, which is naturally related to the temperature and pressure of the O_2 gas at the reaction condition. Here, we calculated the phase diagram for the transition from a clean surface (Figure S4a) to an oxygen-covered surface (Figure S4b). The reaction Gibbs free energy (ΔG) for the transition from a clean surface to an oxygen-covered surface can be calculated as follows:

$$\Delta G = G^{sur}_{O\text{ - cover}} - G^{sur}_{Clean} - \mu_{O_2}$$

where $G^{sur}_{O\text{ - cover}}$ and G^{sur}_{Clean} are the Gibbs free energies for the clean CeO_2(110) surface and the oxygen-covered CeO_2(110) surface, respectively, and are obtained from the DFT calculations. $\mu_{O_2}$is the chemical potential of gaseous O_2. $\mu_{O_2}$is calculated as follows:

$$\mu_{O_2}(T, P) = E_{O_2} + \Delta\mu_{O_2}(T, P)$$

where T is the temperature, P is the pressure of O_2, E_{O_2} is the total energy of O_2 from the DFT calculations. $\Delta\mu_{O_2}(T, P)$ is the change of the chemical potential, which is calculated as follows:

$$\Delta\mu_{O_2}(T, P) = -TS(T, P^0) + RT\ln\frac{P}{P^0}$$

where R is the gas constant, S is the entropy, P^0 is the standard pressure.

As shown in Figure S4c, under the typical experimental condition of T = 500 K and P_{O2} = 0.03 atm, ΔG is significantly greater than 0. This indicates that the transition from a clean surface to an oxygen-covered surface could be not favorable at the reaction condition. In addition, the microkinetic simulation shows that at the steady state, the coverage of the oxygen adsorbed on the Ce site is very low (6.69×10^{-5}), illustrating that the original surface remains predominant under the reaction condition. Therefore, the Ce_{cus} and O_{lat} sites could be the stable basic reaction sites for NH_3-SCR.

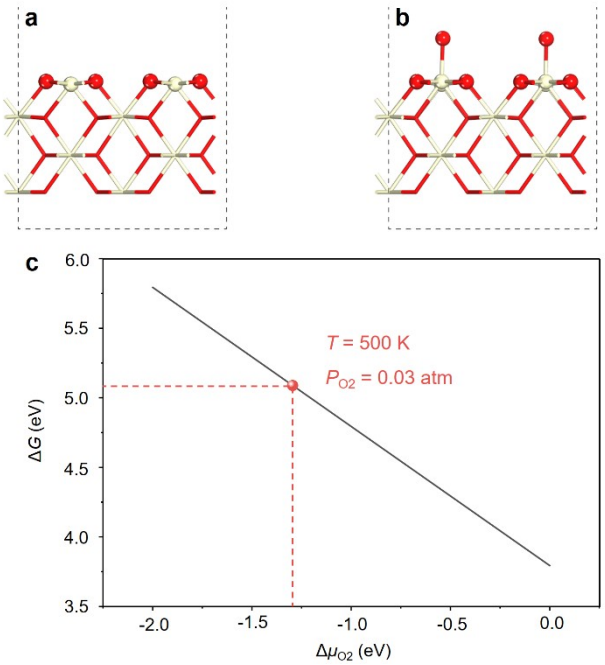

Figure S4. (a, b) Structures of the clean CeO_2(110) surface (a) and the oxygen-covered CeO_2(110) surface (b). (c) The phase diagram for the transition from a clean surface to an oxygen-covered surface.

Table S2. Microkinetic data calculated at the steady state for NH_3-SCR on CeO_2(110), which contain the rate r_i, the reversibility Z_i and the degree of rate control X_{RC} of each step i.[a] The experimental condition for NH_3-SCR on CeO_2, T = 500 K, P_{NH3} = 5.0×10^{-4} atm, P_{NO} = 5.0×10^{-4} atm, P_{O2} = 0.03 atm, P_{N2} = 0.8 atm and P_{H2O} = 0.05 atm was used.[3]

	Step i	E_a / eV	ΔG / eV	k^+	K_{eq}	r / s^{-1} site^{-1}	Z_i	X_{RC}
R1	NH_3+*<->NH_3*	/	0.42	3.00×10^{7}	6.57×10^{-5}	2.15×10^{-2}	1.00	2.26×10^{-7}
R2	NO+*<->ON*	/	0.87	1.98×10^{4}	1.90×10^{-9}	7.36×10^{-9}	1.00	3.79×10^{-17}
R3	NO+O#<->ONO#	/	-0.28	2.26×10^{7}	5.90×10^{2}	2.15×10^{-2}	1.00	7.06×10^{-5}
R4	NH_3*+O#<->NH_2*+HO#	0.41	0.29	7.91×10^{8}	1.07×10^{-3}	2.15×10^{-2}	9.49×10^{-1}	5.13×10^{-2}
R5	NH_2*+ON*<->NH_2NO*+*	0.00	-2.43	1.04×10^{13}	2.99×10^{24}	7.36×10^{-9}	9.86×10^{-16}	3.26×10^{-7}
R6	NH_2*+NO<->NH_2NO*	/	-1.76	1.66×10^{7}	5.23×10^{17}	9.62×10^{-6}	1.07×10^{-17}	4.26×10^{-4}
R7	ONO#+NH_2*<->O#+NH_2NO*	0.26	-0.89	2.47×10^{10}	1.01×10^{9}	2.15×10^{-2}	9.37×10^{-12}	9.54×10^{-1}
R8	NH_2NO*+O#<->NHNO*+HO#	0.06	-0.56	2.59×10^{12}	4.09×10^{5}	2.14×10^{-2}	5.56×10^{-4}	5.15×10^{-7}
R9	NHNO*+HO#<->NHNOH*+O#	0.97	0.85	1.74×10^{3}	2.71×10^{-9}	2.92×10^{-9}	1.08×10^{-1}	-3.61×10^{-10}
R10	NHNOH*+*+O#<->N_2*+HO*+HO#	0.01	-3.18	8.26×10^{12}	1.12×10^{32}	2.92×10^{-9}	3.39×10^{-23}	-4.39×10^{-11}
R11	NHNO*+O#<->N_2O*+HO#	0.42	-1.31	6.33×10^{8}	2.05×10^{13}	6.50×10^{-4}	3.69×10^{-19}	5.17×10^{-5}
R12	N_2O*<->N_2O+*	/	-1.00	1.04×10^{13}	1.19×10^{10}	6.50×10^{-4}	9.63×10^{-1}	9.99×10^{-18}
R13	N_2O*+*<->N_2*+O*	2.20	1.51	7.52×10^{-10}	6.18×10^{-16}	-6.54×10^{-8}	8.13×10^{16}	1.43×10^{-8}
R14	N_2O+#<->N_2O#	/	0.87	1.63×10^{4}	1.56×10^{-9}	6.97×10^{-12}	1.00	-1.66×10^{-18}
R15	N_2O#+*<->N_2*+O#	0.53	-1.83	4.73×10^{7}	3.18×10^{18}	6.97×10^{-12}	4.36×10^{-12}	-5.71×10^{-13}
R16	N_2*<->N_2+*	/	-0.87	1.04×10^{13}	6.37×10^{8}	-6.25×10^{-8}	1.00	1.06×10^{-19}
R17	NHNO*+#<->NHNO#+*	0.00	-3.46	1.04×10^{13}	8.06×10^{34}	2.07×10^{-2}	1.03×10^{-26}	-5.17×10^{-5}
R18	NH_2NO*+#<->NH_2NO#+*	0.00	-1.45	1.04×10^{13}	3.64×10^{14}	1.67×10^{-4}	6.14×10^{-6}	-5.15×10^{-7}
R19	NH_2NO#+O#<->NHNO#+HO#	0.69	-1.83	1.17×10^{6}	3.13×10^{18}	1.67×10^{-4}	2.70×10^{-17}	1.03×10^{-7}
R20	NHNO#+O#<->N_2+O#+HO#	0.65	-1.55	3.19×10^{6}	3.96×10^{15}	2.09×10^{-2}	3.65×10^{-13}	4.76×10^{-6}
R21	HO#+HO#<->H_2O#+O#	0.50	0.17	8.78×10^{7}	1.94×10^{-2}	2.66×10^{-2}	1.00	-1.37×10^{-5}
R22	H_2O#<->H_2O+#	/	0.28	4.35×10^{4}	1.49×10^{-3}	2.66×10^{-2}	9.96×10^{-1}	-3.61×10^{-3}
R23	O_2+#<->O_2#	/	-0.68	2.18×10^{7}	6.68×10^{6}	5.71×10^{-3}	9.98×10^{-1}	-1.72×10^{-3}
R24	O_2#+*<->O#+O*	1.66	1.30	2.11×10^{-4}	7.23×10^{-14}	-4.96×10^{2}	3.73×10^{6}	-7.98×10^{-1}
R25	O*+HO#<->O#+HO*	0.26	-0.34	2.73×10^{10}	2.77×10^{3}	-4.96×10^{2}	1.06	-4.66×10^{-2}
R26	HO*+HO#<->H_2O*+O#	0.39	0.34	1.11×10^{9}	3.73×10^{-4}	-4.96×10^{2}	1.00	-2.41×10^{-4}
R27	O_2#+HO#<->HOO#+O#	0.77	0.43	1.93×10^{5}	4.61×10^{-5}	4.96×10^{2}	4.39×10^{-1}	4.74×10^{-1}
R28	HOO#+*<->O#+HO*	0.83	-0.19	4.68×10^{4}	8.84×10^{1}	6.11×10^{-1}	4.42×10^{-1}	4.56×10^{-4}
R29	HOO#+HO#<->O#+O#+H_2O	0.35	-0.94	2.91×10^{9}	3.05×10^{9}	4.96×10^{2}	6.22×10^{-10}	3.71×10^{-1}
R30	H_2O*<->H_2O+*	/	-0.21	3.78×10^{9}	1.30×10^{2}	-4.96×10^{2}	1.00	-4.81×10^{-4}

[a] * and # represent Ce_{cus} and O_{vac} sites, respectively.

Table S3. Coverages ($\theta(n)$) of key intermediates in NH_3-SCR on CeO_2(110).

Species	$\theta(n)$	Species	$\theta(n)$
*	6.40×10^{-1}	#	4.92×10^{-6}
NH_3*	2.10×10^{-7}	O#	2.54×10^{-3}
NH_2*	1.16×10^{-10}	ONO#	7.49×10^{-3}
NH_2NO*	3.25×10^{-12}	N_2O#	2.31×10^{-19}
NHNO*	4.04×10^{-10}	NH_2NO#	5.59×10^{-8}
NHNOH*	2.17×10^{-19}	NHNO#	2.58×10^{-6}
NO*	6.08×10^{-12}	H_2O#	1.65×10^{-4}
N_2O*	1.67×10^{-15}	HO#	4.66×10^{-3}
N_2*	8.03×10^{-10}	HOO#	3.66×10^{-5}
H_2O*	2.46×10^{-4}	O_2#	9.85×10^{-1}
HO*	3.60×10^{-1}	O*	6.69×10^{-5}

Table S4. Adsorption energy of O_2 on O_{vac} calculated by the PW91 and SCAN functional, respectively.

	PW91	SCAN
E_{ads}	1.42 eV	1.74 eV

Note S3. To assess the accuracy of our kinetic result, we fitted the variation of the production rates for NH_3-SCR with $1/T$ on CeO_2 for NH_3-SCR, which is an important analytical method in catalysis for determining the apparent activation energy of the reaction. The apparent activation energy reflects the intrinsic activation barrier of the kinetically relevant elementary step. As shown in the blue line (Figure S5), at the PW91 level, the apparent activation energy of NH_3-SCR on CeO_2 is about 37.95 kJ/mol, which is slightly higher than the experimental value (24.8 ± 0.6 kJ/mol[7]). The discrepancy of the theoretical and experimental apparent activation energies can be attributed to the accuracy of kinetic parameters for the rate-determining step of NH_3-SCR on CeO_2.

According to the microkinetic analysis, the rate-determining step of NH_3-SCR on CeO_2 is the formation of NH_2NO, i.e., $*NH_2 + ONO\# \rightarrow *NH_2NO + O\#$. The reaction rate can be expressed as: $r = k^+\theta(*NH_2)\theta(ONO\#)(1-Z)$, where k^+ is the rate constant, $\theta(*NH_2)$ is the coverage of NH_2 on Ce site, $\theta(ONO\#)$ is the coverage of NO on the lattice oxygen (O_{lat}), and Z is the reversibility. Given Z is negligible, it can be ignored in this context. Thus, k^+, $\theta(*NH_2)$ and $\theta(ONO\#)$ are the three main factors determining the apparent activation energy. Here, k^+ is determined by the energy barrier of this step, which comes from the relatively accurate DFT calculation. $\theta(*NH_2)$ is determined by the NH_3 adsorption/dissociation and the competitive adsorption of other species. The energy information for NH_3 adsorption/dissociation are also reasonably accurate from DFT calculations. Additionally, the Ce sites are relatively vacant due to the weak adsorption of other competitive reactants (e.g., E_{ads} = -0.13 eV for O_2 and E_{ads} = -0.23 eV for NO), making $\theta(*NH_2)$ relatively reliable in the microkinetic simulation. In contrast, $\theta(ONO\#)$ is primarily determined by the coupling between NO and the O_{lat} and by the competitive adsorption of species like O_2 on O_{vac}. The energy data for the ON-O_{lat} coupling step are relatively accurate from DFT calculations. While, the PW91 functional tends to overestimate the O-O bonding energy in O_2 molecule, leading to an underestimation of the adsorption energy of O_2 on O_{vac} and thus influencing the $O_2\#$ coverage. This, in turn, affect $\theta(ONO\#)$ due to the competitive adsorption, which potentially affect the accuracy of the microkinetic model.

To further verify the above conjecture, we recalculated the O_2 adsorption on O_{vac} using the more accurate SCAN functional. As shown in Table S4, the O_2 adsorption energy on O_{vac} is about -1.74 eV, which is more negative than the value obtained from the PW91 functional (-1.42 eV). Incorporating this more accurate O_2 adsorption energy in the microkinetic simulation, we observed that a subsequent adjustment of the apparent activation energy (see the red line in Figure S5). The revised apparent activation energy is about 24.91 kJ/mol, which is closer to the experimental value (24.8 ± 0.6 kJ/mol[7]). This optimization suggests that improving the quantitative accuracy of the microkinetic model is useful and important in our system (see the detailed kinetic

data in Table S2 and Table S3).

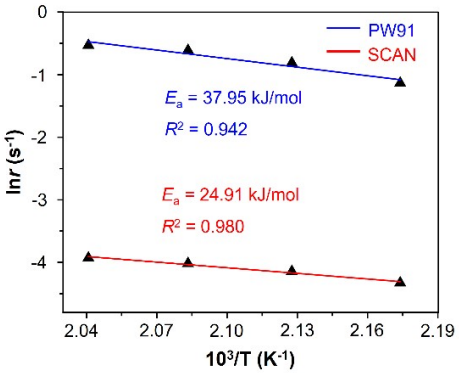

Figure S5. Arrhenius plot for NH_3-SCR reaction resulting from the microkinetic simulation, in which the blue and red lines represent the O_2 adsorption energy from the PW91 and SCAN functional, respectively.

References

1. H. Yuan, N. Sun, J. Chen, J. Jin, H. Wang, P. Hu, *ACS Catal*. 2018, **8**, 9269-9279.
2. Q. L. Tang, Q. J. Hong, Z. P. Liu, *J. Catal.* 2009, **263**, 114-122.
3. J. Han, J. Meeprasert, P. Maitarad, S. Nammuangruk, L. Shi and D. Zhang, *J. Phys. Chem. C* 2016, **120**, 1523-1533.
4. J. Chen, M. L. Jia, P. Hu and H. F. Wang, *J. Comput. Chem.* 2021, **42**, 379-391.
5. J.F. Chen, M.L. Jia, Z.Z. Lai, P. Hu and H. F. Wang, *J. Chem. Phys.* 2021, **154**, 024108.
6. J.F. Chen, Y. Mao, H.F. Wang and P. Hu, *ACS Catal.* 2016, **6**, 7078-7087.
7. M. Iwasaki, K. Dohmae, Y. Nagai, E. Sudo and T. Tanaka, J. Catal. 2018, **359**, 55-67.